ASSESSMENT OF PANCREATIC ISLET TRANSPLANTS USING *IN VIVO* BIOLUMINESCENCE IMAGING

By

John M. Virostko

Thesis

Submitted to the Faculty of the

Graduate School of Vanderbilt University

in partial fulfillment of the requirements

for the degree of

MASTER OF SCIENCE

in

Biomedical Engineering

December, 2003

Nashville, Tennessee

Approved

E. Duco Jansen

Alvin C. Powers

ACKNOWLEDGEMENTS

I would like to give special thanks to my parents for their guidance and support throughout my education.

I would also like to thank Professor Duco Jansen and Dr. Al Powers, for guidance in this research and preparation of this thesis.

My gratitude also to Greg Poffenberger, Dr. Michael Fowler, and Dr. Zhongyi Chen for assistance with surgeries.

TABLE OF CONTENTS

Page

LIST OF TABLES

LIST OF FIGURES

LIST OF SYMBOLS

Symbol	Definition	Units
n	Index of Refration	-
c	Speed of Light in a Vacuum	m/s
v	Speed of Light in Medium	m/s
λ	Wavelength	m
I	Radiant Intensity	W/m^2
ξ	Molar Extinction Coefficient	$M^{-1}m^{-1}$
δ	Penetration Depth	m
μ_a	Absorption Coefficient	m^{-1}
μ_s	Scattering Coefficient	m^{-1}
g	Anisotropy Factor	-
μ_s'	Reduced Scattering Coefficient	m^{-1}
μ_{eff}	Effective Attenuation Coefficient	m^{-1}
δ_{eff}	Effective Penetration Depth	m^{-1}
S	Rate of Heat Generation	W/m^3
L	Radiance	W/m^2sr

CHAPTER I

INTRODUCTION

Pancreatic islet transplantation shows potential for the treatment of type 1 diabetes mellitus. The recent success of transplants using the Edmonton Protocol indicates that islet transplantation is indeed a feasible treatment for type 1 diabetes [1]. Advances in islet isolation and immunosuppression have greatly improved the success of these transplants. However, the number of islets needed to overcome diabetes presents a major obstacle precluding islet transplantation from being adopted as a routine treatment. Most patients require islets isolated from at least two pancreata. The supply of islets from organ donors falls well short of the amount needed to treat the estimated 17 million type 1 diabetics in the United States [2]. The survival rate of transplanted islets is unknown; it is thought that many islets die post transplantation without engrafting. Thus a significant amount of research is focused on preserving or increasing islet mass post transplantation. However, there is currently no suitable method of non-invasively measuring islet mass. Islet mass is commonly estimated from insulin secretion following glucose tolerance testing. However, this method assesses islet function, which does not necessarily correlate with islet mass. Morphometric analysis of histological sections of islet grafts can be used to measure islet mass, but requires removal of the organ containing the islets, preventing any sequential studies. Additionally, this morphometric analysis is difficult to perform when islets are scattered, as they are when embolizing in the liver.

This study seeks to develop *in vivo* bioluminescence imaging (BLI) as a method to quantify the number of islets surviving post transplantation. The firefly luciferase reporter gene was inserted into the islets by means of an adenovirus to provide a means of tracking islets by light emission. These pancreatic islets were then transplanted beneath the renal capsule or infused into the portal vein of NOD-SCID mice. The light emitted from these bioluminescent islets was imaged and quantified using an ultra-sensitive CCD camera. As the mice bearing the islet transplant could be imaged repeatedly, bioluminescence (and thus islet mass) could be tracked temporally.

In order to validate the method of bioluminescence imaging for assessing transplanted islets mass, the factors that influence light emission were examined. The amount of light

reaching the camera is determined by the optical properties of the tissue through which the light must pass and the geometry of the sample relative to the imaging system. Constant emission, isotropic light emitting beads with spectral emission similar to the luciferase reaction were implanted at the renal capsule or within the liver of NOD-SCID mice. These beads provided a constant source of luminescence from a location used for islet transplants. These bead-implanted mice were used for investigation of the tissue optics governing light transmission from the islet grafts to the camera aperture. The effects of wound healing, mouse positioning, and light attenuation by tissues overlying the islet grafts were determined by imaging these bead-implanted mice.

History of Islet Transplantation

While the current success of islet transplantation has only recently established it as an effective clinical treatment for type 1 diabetes, the motivation behind islet transplantation is over a century old. The link between diabetes and the pancreas was first discovered in 1889 in studies of a pancreatectomized dog which developed acute hyperglycemia and glucosuria [3]. Three years later Minkowski successfully transplanted autologous sections of the pancreas into a pancreatectomized dog [4]. The first clinical implementation of pancreas transplantation was performed in 1894 on a patient with diabetes ketoacidosis. Three pieces of a sheep pancreas were transplanted subcutaneously in a 13-year-old recipient. The patient showed temporary improvement in glucosuria before his death three days later from autoimmune rejection of the xenograft [5]. The first successful reversal of hyperglycemia was accomplished by Banting, et al, in 1922 by treatment with bovine pancreatic extract [6]. Purified insulin production commenced the following year. Insulin therapy became the definitive treatment for diabetics.

Despite the success of insulin injections in overcoming hyperglycemia, they fail to prevent a number of the chronic ailments associated with diabetes. Renal failure, blindness, heart disease, neuropathy, and atherosclerosis continue to afflict diabetics despite insulin therapy [2]. The ability of the islets of Langerhans to exquisitely control carbohydrate metabolism cannot be fully accomplished by insulin injections alone, primarily due to lack of real-time feedback and consequently significant swings in blood glucose levels. These shortcomings of insulin renewed interest in pancreas transplantation. The first successful clinical pancreatic transplant was performed in 1967 [7]. The patient's hyperglycemia was reversed until

complications later forced removal of the graft. Later attempts at pancreas transplantation proved more successful. Over 1000 pancreas transplants are now performed annually, with a success rate of 70% [8]. A successful pancreatic transplantation renders the recipient free from any exogenous insulin injections with normal blood glucose and HbA_{1c} levels [9]. The chronic effects of diabetes are lessened: diabetic retinopathy is partially reversed [10] and native renal structure is restored ten years post implant [11]. Transplant recipients report a higher quality of life [12].

Pancreatic transplants have demonstrated some benefits over insulin injections for the alleviation of chronic ailments and improved quality of life. Patient survival rates one year after pancreatic transplantation surpass 90% [13]. However, pancreatic transplantation has disadvantages. Successful transplantation typically requires simultaneous transplantation of both the pancreas and kidneys. This surgery is plagued by complications resulting in prolonged hospital stays and repeat surgeries [14]. This in turn results in high costs. The diabetes community has thus begun focusing on transplanting solely the pancreatic islets. The majority of the pancreas is an exocrine digestive gland; only 1-2% of the pancreas is composed of the islets that contain insulin-producing β-cells. Transplanting solely the islets of the pancreas is a much less invasive procedure expected to be much safer and less costly to the patient [9]. Pancreatic islets removed from cadaver pancreata can be isolated using collagenase enzyme extracts to yield purified islets [14]. The first successful transplantation of islets into rats showed promise that it would soon become the definitive treatment for type 1 diabetes [15]. However, four years later the first clinical trial on seven diabetics using corticosteroid immunosuppression failed to render any of the seven patients insulin independent [16]. Success came with islet autotransplantation on patients undergoing a total pancreatectomy and infused with their own islets [17]. Without the need for any immunosuppressive drugs these patients with islet autografts delayed the onset of diabetes for over a decade [18]. Results with allografts – transplants from a different individual of the same species - have proven less promising. Of the 237 adult islet allotransplants reported to the International Islet Transplant Registry (IITR) by December 31, 2001 fewer than 12% remained free from insulin injections one year following transplantation [19].

The failure of allotransplants to succeed while autotransplants thrived focused attention on the high levels of immunosuppressive drugs given to patients with allografts. The potent

immunosuppressive drugs tacrolimus (FK) and cyclosporine (CSA), regularly given to organ transplant recipients to prevent rejection, were found to be toxic to islets, causing distinct morphological damage to beta cells [20]. In 2000 researchers at the University of Alberta reported a modified protocol to treat seven patients with type 1 diabetes. The equivalency of two donor pancreata were infused into patients via a percutaneous transhepatic portal embolization. Transplant recipients were given a glucocorticoid-free immunosuppressive regimen of sirolimus, tacrolimus, and daclizumab. All seven patients attained insulin independence following transplant and maintained freedom from insulin injections one year post op [1]. The modified protocol has subsequently been called the Edmonton Protocol. A major multi-center study is now being conducted to test the feasibility of the Edmonton Protocol. A 90% success rate was recently reported by three participating centers with extensive experience in islet isolation [21].

Bioluminescence

Bioluminescence manifests in nature in a variety of forms. An assortment of organisms emit visible light, ranging from the ubiquitous firefly to marine bacteria. Organisms exhibit bioluminescence for a variety of reasons: courtship and mating signaling, luring prey, defense, camouflage, and in response to stress [22]. This natural phenomena has been harnessed for use in research as an optical reporter tool.

Bioluminescence results from interaction of the luciferase enzyme with the substrate luciferin in the presence of oxygen. A wide range of luciferase enzymes exist, each of which catalyze the oxidation of luciferin with corresponding release of photons of light. The luciferase enzyme found in the firefly, *Photinus pyralis*, catalyzes bioluminescence in the presence of ATP through the following reaction [23].

$$\text{Luciferase} + \text{Luciferin} + \text{ATP} + O_2 \xrightarrow{Mg^{2+}} \text{Luciferase-Luciferin} + \text{AMP} + PP_i \quad (1)$$

$$\text{Luciferase-Luciferin} + \text{AMP} + O_2 \longrightarrow \text{Oxyluciferin}^* + CO_2 + \text{AMP} \quad (2)$$

$$\text{Oxyluciferin}^* \longrightarrow \text{Oxyluciferin} + h\nu \quad (3)$$

In the presence of oxygen, magnesium, and ATP, the reaction of the luciferase enzyme with the substrate luciferin yields an electronically excited oxyluciferin. The return of oxyluciferin to its ground state is accompanied by the release of a single photon [24]. Thus, in the presence of

excess luciferin, oxygen, and ATP, the number of photons emitted is proportional to the number of molecules of luciferase present [25].

Firefly luciferase was first purified and characterized in 1978 by Gates, et al. [26]. The cDNA for firefly luciferase was then cloned in 1987 for use as an optical reporter [27]. This luciferase cDNA was inserted into monkey kidney cells and incorporated into the cell's DNA. The luciferase enzyme was produced and sequestered in the peroxisomes of cells; subsequent luciferin entry into the cell catalyzed a bioluminescent reaction [28]. Since then luciferase has been used as an optical reporter gene in a wide variety of applications. Luciferase has been used to study protein site-specific secretion, protein targeting, transgenic promoter activation, ATP and free Ca^{2+} concentrations, and the immune response [22]. A notable application of bioluminescence imaging is the visualization of gene expression in individual cells in real time. Real time gene expression was first performed by tagging shuttle vectors with luciferase DNA and checking for functional coding sequences by visualizing luminescence on photographic film [29]. Since then, luciferase imaging has been used to monitor gene expression in a wide range of studies.

Bioluminescence imaging has long been used as a means of imaging cells *in vitro*. However, bioluminescent signals from sources deep within an animal are subject to attenuation by tissues overlying the source, previously preventing bioluminescence imaging on whole live animals. The recent advent of ultra-sensitive charge coupled device (CCD) cameras capable of single photon counting has enabled *in vivo* imaging of bioluminescence. CCDs consist of an array of capacitors that accumulate electric charge proportional to the light intensity at that location in the array. The liquid nitrogen-cooled, back-thinned, back-illuminated CCD camera has a quantum efficiency (QE) of 85%, an order of magnitude better than the QE of intensified CCDs previously used in bioluminescent imaging [30]. Cooling the camera with liquid nitrogen reduces the dark noise on the chip to near negligible levels. These advances in CCD detector sensitivity now allow *in vivo* bioluminescence imaging (BLI) of luciferase expression. Gene expression in mice can be tracked externally by tagging viral vectors with the luciferase gene and imaging light emission following luciferin injection [31]. BLI has been used to non-invasively track tumor metastasis, with light emission directly related to tumor volume [32]. Other BLI applications include transplant studies, *in vivo* gene expression studies using a variety of transgenic animal models, and host-pathogen interactions [31].

Optical imaging holds several advantages over traditional imaging modalities such as MRI or CT. The CCD cameras used for optical imaging cost less than MRI and CT equipment. Imaging times are shorter and multiple animals can be imaged at once. Operation of CCD cameras is typically easier than that of other modalities, permitting use by a non-specialist. Optical imaging also permits quantification of metabolically active cells and permits the visualization of gene expression [30]. Lastly, optical imaging is inherently more sensitive than any other imaging modality. For the purpose of this study, bioluminescence imaging is superior to other optical methods, such as fluorescence. Fluorescence requires excitation light to stimulate light emission; bioluminescence is the product of a reaction requiring no excitation light. The wavelengths of light needed for fluorescence excitation fall in the blue spectrum of light, wavelengths that are highly attenuated by blood and tissue. In contrast, the emission spectrum of bioluminescence is broad, ranging from 500 to 700 nm, with a peak around 560 nm [30]. These higher wavelengths are attenuated less by tissue; thus bioluminescence can be detected from much deeper sources (several centimeters) than fluorescence. Furthermore, bioluminescence is not subject to bleaching and auto-fluorescence issues that can skew fluorescence measurements. Fluorescence measurements must take into account the number of excited cells as well as intensity of excitation light. Quantification of bioluminescence is easier: light emission is directly proportional to the amount of luciferase, which in turn is proportional to the number of cells [30].

Tissue Optics

Detailed knowledge of tissue optics is essential for quantitative interpretation of measure bioluminescence signals. Photon-counting measurements must take into account the tissue optics governing light transmission from the luminescent source to the imaging system. The propagation of light through biological tissue is governed by the interaction between tissue optical properties and sample geometry. The movement of photons through a turbid biological media is influenced by scattering and absorption events within the tissue and reflection and transmission events at tissue boundaries. These phenomena have been studied in depth and can now be mathematically analyzed and modeled.

Reflection of light occurs at the boundary between media with different optical properties. The amount of light reflected depends on the angle of incident light and the index of

refraction of each medium. Index of refraction is a measure of the speed of light travel through a medium. Index of refraction, n, is given as the ratio of the speed of light in a vacuum to the speed of light within the media,

$$n = \frac{c}{v} \tag{4}$$

where c is 3 * 10^8 m/s. The specular reflection at the boundary between two media is given by Fresnel's equation,

$$r = \frac{1}{2}\left[\frac{\tan^2(\theta_1 - \theta_2)}{\tan^2(\theta_1 + \theta_2)} + \frac{\sin^2(\theta_1 - \theta_2)}{\sin^2(\theta_1 + \theta_2)}\right] \tag{5}$$

in which θ_1 is the angle of incidence and θ_2 is the angle of transmittance. For beams normal to the surface ($\theta_1 = 0$) this equation reduces to

$$r = \frac{(n_1 - n_2)^2}{(n_1 + n_2)^2} \tag{6}$$

where n_1 is the incident index of refraction and n_2 is the index of refraction of the tissue medium. For a typical tissue air (n = 1.0) tissue (n = 1.33) interface, the reflection is 2%. Reflection is maximized in a phenomenon known as total internal reflection, in which all light is specularly reflected and no light transmission occurs. Total internal reflection occurs when the incident light occurs at an angle greater than some critical angle:

$$\theta_c = \arcsin\left(\frac{n_1}{n_2}\right) \tag{7}$$

Reflection at tissue boundaries decreases the total amount of light transmitted into the tissue initially (known as specular reflectance) as well as at subsequent tissue boundary interactions (diffuse reflectance).

Upon entering a biological medium, protons can be absorbed by the tissue components and converted to heat, catalyze a chemical reaction, or be released as fluorescence emission. This absorption of light by tissue is utilized in many biomedical optics applications, including photodynamic therapy, photothermal ablation, and diagnostic spectroscopy [33]. Molecules that absorb light are known as chromophores; for visible light hemoglobin and melanin are the principle chromophores. Light absorption is governed by the probabilistic exponential decay of Beer's law. Beer's law depends on the concentration of the absorbing medium, c, and the

molecular absorption coefficient, $\xi(\lambda)$, a wavelength dependent property. Beer's law gives the loss of initial light intensity, $I_{0,}$ as a function of tissue depth:

$$\frac{dI}{dz} = -c\xi(\lambda)I_0 \tag{8}$$

Molecular absorption coefficient and concentration are typically combined in one parameter, μ_a, the wavelength dependent absorption coefficient. The mean free path, also known as penetration depth, is equal to the inverse of the absorption coefficient. This depth is the point at which 63% of the incident light has been absorbed.

Photons are scattered in media with spatial fluctuations in density and refractive index, n, resulting in changes in photon path direction. In biological tissue, discrete particles such as cell membranes, nuclei, collagen, or other cellular microstructure can cause photon scattering. Two forms of scattering can occur: elastic scatter, in which no photon energy is lost; and inelastic scatter, in which some photon energy is transferred to the scattering molecule. Inelastic scatter results in the Stokes shift, a phenomena exploited in Raman spectroscopy. Elastic scatter simply results in the impinging photon redirected in a new path. Scattering is treated much like absorption, a probabilistic approach using exponential decay. The scattering coefficient, μ_s, gives the probability of a photon being scattered per infinitesimal distance.

The direction of photon scattering is a complex estimate governed by a phase function. Assuming isotropic tissue optical properties, for a given photon moving in direction $\vec{s}$ scattered to new direction $\vec{s}'$

$$p(\vec{s},\vec{s}') = \frac{1}{4\pi} \tag{9}$$

In reality, light scattering in biological tissue is not isotropic. The directional dependence of photon scatter is quantified by an anisotropy factor, g, which correlates to the cosine of the expected scattering angle. Integrated over an entire sphere:

$$g = \int_{4\pi} p(\vec{s},\vec{s}')(\vec{s}\cdot\vec{s}')d\omega \tag{10}$$

Values of the anisotropy factor range from 1, indicating completely forward scatter, to –1, indicating completely backward scatter. For biological tissue, g ranges from 0.7 to 0.99, indicating forward dominated scatter. The contribution of the anisotropy factor is included in the reduced scattering coefficient:

$$\mu_s' = (1-g)\mu_s \tag{11}$$

This reduced scattering coefficient, μ_s', is combined with the absorption coefficient into the effective attenuation coefficient:

$$\mu_{eff} = \sqrt{3\mu_a\left(\mu_a + \mu_s'\right)} \tag{12}$$

This can then be used to calculate the effective penetration depth:

$$\delta_{eff} = \frac{1}{\mu_{eff}} \tag{13}$$

This distance represents the distance required for intensity to be reduced to 37% of the initial intensity.

The light transport equation provides a general solution for light propagation in turbid media:

$$\frac{dL(r,\vec{s})}{ds} = -\mu_a L(r,\vec{s}) - \mu_s L(r,\vec{s}) + \mu_s \int_{4\pi} p(\vec{s},\vec{s}')L(\vec{r},s)d\omega + S(r,\vec{s}) \tag{14}$$

Simply put, the gradient of the radiance at point r in direction $\vec{s}'$ equals the (negative) loss due to absorption, minus the loss due to scattering, plus the gain from scattering, plus the power source at point r in direction $\vec{s}'$. This theory assumes steady state, homogenous optical properties, isolated particles, and no polarization or collimation. Tissue is approximated as a finite plane parallel slab with finite thickness. While the light transport equation is not easily solved, a number of mathematical models of the light transport equation exist. Monte Carlo simulation, Adding-Doubling Method, Diffusion Approximation Theory, and Kubelka-Munk Theory each provide a solution method applicable with unique boundary conditions [33].

Determining the optical properties of biological tissue poses a difficult problem. *In vivo* optical properties are difficult to measure, while *in vitro* optical properties are not known with great accuracy due to the shortage of adequate techniques [33]. For optically thin tissue samples with single scattering events, light absorbed and scattered can be directly measured using a reflection and transmission detector. For thicker samples a double integrating sphere is employed. A sample is placed between two spheres and a light source is shone on the tissue. One detector measures diffuse reflectance while another measures light transmission. The reflection and transmission values at each wavelength can then be used to inversely solve the

light transport equation iteratively to find the fundamental optical properties. Optical properties of an *in vitro* tissue sample can also be determined using the 'added absorber' method. An optical absorber is added in known concentrations to a bulk tissue, increasing absorption but not affecting scattering. Absorption and scattering coefficients can be estimated by plotting μ_{eff} versus absorber concentration [34]. *In vitro* measurements of optical properties are not necessarily valid for the same tissue *in vivo*. Biochemical and morphological changes accompanying tissue excision, temperature fluctuations, and changes in hydration can all affect optical properties of biological tissue [35]. A fiber optic probe can be used to measure the spatial distribution of fluence in a tissue *in vivo*. The fluence mapping can be modeled to determine absorption and scattering coefficients. Diffuse reflectance measurements can be performed non-invasively using a fiber optic probe; the spatial distribution of these measurements can be modeled and used to estimate optical properties. Although less refined than the photometric measurements outlined above, photothermal techniques for measuring optical properties are under development. Pulsed photothermal radiometry measures the radiative heat flux from an irradiated tissue to indirectly estimate optical properties of strongly absorbing tissues. Photoacoustic spectroscopy (PAS) measures acoustic pressure waves emitted from irradiated tissue. The amplitude and phase of the acoustic wave can then be used to estimate optical properties.

CHAPTER II

ASSESSMENT OF PANCREATIC ISLET TRANSPLANTS USING *IN VIVO* BIOLUMINESCENCE IMAGING

Abstract

Pancreatic islet transplantation is a promising treatment for type 1 diabetes. However, current efforts to study islet transplantations are hampered by the lack of a non-invasive method of imaging islets and quantifying islet mass post transplantation. Transplanted pancreatic islets can be imaged and quantified non-invasively using *in vivo* bioluminescence imaging (BLI). Pancreatic islets transfected with the firefly reporter gene, luciferase, emit light that can be quantified using photon-counting measurements. Pancreatic islet number is linearly related to light emission both *in vitro* and *in vivo*. Application of bioluminescence imaging for this application can be greatly enhanced by relating light emission to the number of islets surviving post-transplantation. Determining this relationship requires detailed knowledge of the factors that influence photon-counting measurements. Bioluminescence was modeled using constant light emitting phosphorescent beads implanted at the two common sites of islet transplantation: the renal capsule and liver. This model was used to quantify light attenuation by tissues overlying the islet transplantations. The ratio of implanted light emission to *in vitro* light emission was found to be .2394+/- 0.0261 for renal implantation and 0.0645 +/- 0.0140 for hepatic implants. Mathematical modeling of light propagation using Monte Carlo simulation is in excellent agreement with these experimental results. Monte Carlo modeling yields an *in vivo* to *in vitro* luminescence ratio for renal and hepatic sources to be 0.2860 and 0.0495, respectively. Surgical artifacts were found to influence bioluminescence measurements. Surgical scar tissue leads to lower light emission the week immediately post-op, but this attenuation is negligible two weeks after surgery. The orientation of the subject also influences quantification of bioluminescence. Rotation of 50 degrees from flat can lead to a 73% decrease in light transmission for renal implants and 52% decrease for hepatic implants. The rate of luminescence decrease with increasing angle depends on the surface light is projected upon. Flatter surfaces lead to a slower decrease in luminescence while higher curvature leads to more rapid decrease in

luminescence. Spot size of bioluminescence was found to increase with increasing tissue depth. The spot size of hepatic implants was found to be 17% larger than renal implants, as measured by full width at half maximum measurements. Constant light emission modeling of transplanted islet bioluminescence permits quantification of actual islet number from photon counting measurements and insight into factors which influence these measurements.

Introduction

Pancreatic islet transplantation is showing promising results in the treatment of type 1 diabetes. The success of islet transplants using the Edmonton Protocol has given hope that transplantations may one day replace insulin therapy as the definitive treatment for type 1 diabetes [1]. The success of the Edmonton Protocol is now being tested in a large multi-center trial [21]. Islet transplantation not only frees diabetics from daily insulin injections, but may also ameliorate some of the chronic pathologies associated with diabetes [2]. The ability of transplanted pancreata to exquisitely regulate blood glucose levels results in partial reversal of diabetic retinopathy [10] and restoration of native renal structure [11].

Despite advances in immunosuppression and islet isolation utilized by the Edmonton Protocol, islet transplantation is not ready to be adopted as a routine clinical treatment for type 1 diabetes. One major obstacle facing islet transplantation is a shortage of islets. Successful reversal of diabetes requires transplantation of a large quantity of islets, typically the equivalent of two pancreata. The supply of islets available for transplant falls well short of the amount needed to treat the estimated 17 million type 1 diabetics in the United States [2]. The need for immunosuppressive therapy following transplantation is another complication facing islet transplantation. The side effects of immunosuppressive medications can prove worse than the effects of diabetes.

The challenge is now to successfully reverse diabetes while transplanting fewer islets. Considerable research efforts are currently underway to sustain or increase islet mass post transplantation. However, these efforts are hampered by the lack of an adequate method of non-invasively quantifying islet mass post transplantation. Current methods of estimating islet mass are insufficient. Insulin secretion following glucose challenge gives insight into islet function, but not necessarily islet mass. Morphometric analysis of excised islet grafts requires sacrificing the animal, preventing sequential measurements. While useful for islets transplanted beneath the

renal capsule in rodents, morphometric analysis proves difficult for islets scattered throughout the liver, the site of human islet transplantation.

This study investigates the use of *in vivo* bioluminescence imaging (BLI) to track transplanted pancreatic islet mass. Pancreatic islets were transfected with a replication-deficient adenovirus carrying the luciferase reporter under control of a constitutive CMV promoter. The oxidation of luciferin by the luciferase enzyme generates bioluminescence in the presence of ATP and oxygen [23]. These bioluminescent islets were transplanted into the renal capsule or liver of NOD-SCID mice, an immune deficient mouse model that accepts xenografts. The light emission from islet grafts could then be imaged and quantified by an ultra-sensitive CCD camera [31].

Correlation of light emission to islet mass must take into account the factors that influence light transmission from the bioluminescent source to the CCD camera aperture. Light transmission is determined by the optical properties of the tissue through which the light passes. Constant emission, isotropic light emitting beads with spectral emission similar to the luciferase reaction were implanted beneath the renal capsule or liver of NOD-SCID mice. These beads serve as a model of islet bioluminescence, providing a constant light source from the location of the islet grafts. The luminescent beads provide a constant, known light intensity that is reliable and reproducible, allowing for validation of the imaging system. In contrast, bioluminescent islets are subject to biological variability. Islet light emission depends on the health and size of the islets and survival of islets post transplantation. The constant bead light emission was used to quantify the variability inherent in bioluminescence imaging. The effects of wound healing, mouse positioning, and light attenuation by tissues overlying the islet grafts were determined by imaging these bead-bearing mice. These factors must be taken into account when correlating light emission to islet mass. These findings hold important clues for quantitative interpretation of bioluminescence imaging applicable to any study involving quantification of bioluminescence.

Materials & Methods

Animal Model

NOD-SCID mice were obtained from Jackson Laboratories (Bar Harbor, Maine). The NOD-SCID strain is homozygous for the severe combined immune deficiency (SCID) spontaneous mutation, characterized by an absence of functional T cells and B cells. The NOD-SCID strain accepts allografts with no immune rejection response. NOD-SCID mice do not become diabetic or develop insulitis.

Mouse Islet Isolation

The splenic portion of a mouse pancreas was dissected and infused with 3 ml of collagenase P (Roche Molecular Biochemicals, Indianapolis, IN) in Hanks buffered saline (0.6 mg/ml) through the bile duct. Groups of two pancreata were then digested in 6.7 ml of collagenase P (0.6 mg/ml) for 4-5 minutes at 37°C using a wrist action shaker. Some islets were then handpicked under microscopic guidance. Others were purified by histopaque gradient centrifugation and washed 3 times with 10 mM PBS containing 1% mouse serum. Islets were suspended in 30 μL of 10 mM PBS with 1% mouse serum solution.

Human Islet Isolation

Human pancreatic islets were obtained from Dr. David Harlan at NIDDK/NIH and from the JDRFI Islet Distribution Network. Islets were isolated from the cadaver of human organ donors and placed on ice (cold ischemia time < 8h). Islets were digested with a 4°C solution of Liberase HI (Roche Molecular Biochemicals, Indianapolis, IN) injected into the pancreatic ducts coupled with mechanical agitation by shaking. Islets were purified from other pancreatic fragments by density gradient separation. Islets were shipped on ice the same day by overnight courier.

Islet Luciferase Transfection

Islets were cultured in RPMI 1640 (Invitrogen, Carlsbad, CA) with 10% Fetal Bovine Serum (Invitrogen, Carlsbad, CA) and 11mM glucose. Islets were infected with an adenovirus (MOI = 1000) expressing the dual reporter genes luciferase and green fluorescence protein

(GFP). They were then placed in cell culture for 12 hours. Islets were suspended in 30 μL of 10 mM PBS with 1% mouse serum solution.

Kidney Islet Transplantation

Mice were anesthetized with an intraperitoneal injection of 50 mg/kg b.w. sodium pentobarbital (Abbot Laboratories, Chicago, IL). The left flank was then shaved, prepped with ethanol, and draped in sterile fashion. A left flank incision overlying the kidney was performed. The left kidney was then exposed and irrigated with saline. The islet suspension (30 μL) was injected between the renal capsule and parenchyma of the kidney using a 23-gauge butterfly needle. The needle was withdrawn and the insertion point was cauterized. The wound was closed with black subcutaneous sutures (Prolene, Ethicon, Somerville, NJ) and aluminum skin staples (Autoclips, 9 mm size, Clay Adams, Parsippany, NJ).

Liver Islet Transplantation

Mice were anesthetized with an intraperitoneal injection of 50 mg/kg b.w. sodium pentobarbital. The abdomen was then shaved, prepped with ethanol, and draped in sterile fashion. A lateral incision was made in the abdomen above the liver. Islets were infused into the portal vein via PE10 tubing attached to a 30-½ gauge needle. Slight pressure was applied to the insertion point to stop blood loss. The abdominal incision was closed with subcutaneous sutures and skin staples, as described above.

Bioluminescence Imaging of Islets

Bioluminescence imaging was performed using a back thinned, back illuminated charge coupled device (CCD) camera with a 1300x1340 pixel chip (Roper Scientific, Trenton, NJ). Prior to imaging, the camera chip was cooled to -90°C by the addition of liquid nitrogen. A one-millisecond background image was taken to find the background readout noise on the chip. The background image was subtracted from the bioluminescence image to remove background noise. On chip binning of 5 was used for all images to increase signal to noise ratio. Twenty-five pixels (a 5 x 5 square) were combined to generate one pixel. Image integration time was 4 minutes. An overlay image (black and white picture) was taken with a light inside the imaging chamber turned on to illuminate the subject. The luminescence image with peak intensity was used for

image analysis with Metamorph software (Version 4.6r6, Universal Imaging Corporation, Downingtown, PA). Using Metamorph, regions of equal area were drawn around the region of interest (ROI). Luminescence was quantified by summing pixel intensities within the region to yield integrated intensity.

In Vitro Bioluminescence

Islets were preserved in 30 μL of 10 mM PBS with 1% FBS (Invitrogen, Carlsbad, CA) and kept on ice prior to imaging. Islets were then placed in 6 well plates with 100 μl of PBS. The bioluminescence substrate D-Luciferin (Promega, Madison, WI) was added in excess (10 μL of 0.15 mg/ml concentration) to each well. The well plate was placed in the light tight box of the camera system. Bioluminescence was imaged by a four-minute exposure taken with the CCD camera. Another four-minute exposure image was taken following the first, in order to capture the peak in luciferase activity. For in vitro luminescence, the peak luminescence always occurred in the initial 4 minutes following substrate addition.

In Vivo Bioluminescence

Mice were anesthetized prior to imaging with an intraperitoneal injection of 50 mg/kg b.w. sodium pentobarbital. The hair overlying the islet graft was shaved to reduce light scattering. The substrate D-luciferin dissolved in sterile de-ionized water was added by intraperitoneal injection of 150 mg/kg b.w. Mice were secured to a black felt pad using Velcro to minimize any motion artifacts during imaging. This pad was then placed in the light tight imaging chamber. A bioluminescence image with four minute exposure time was taken, followed by another four minute exposure image. The peak luminescence image for *in vivo* bioluminescence was typically the second image taken.

Luminescent Beads

Luminescent beads were obtained from Mb-Microtec (Bern, Switzerland). These beads consist of glass capillaries (0.9 mm diameter and 2 mm long) filled with tritium (a β-emitter with a half life of over 10 years) that excites a phosphor and emits constant intensity light. The spectral emission of these beads was measured using a fiber optic probe attached to a spectrometer (Ocean Optics Inc., Dunedin, FL) equipped with a 360 nm cutoff filter. Spectral

emission of a single bead within a centrifuge tube was measured with one-second integration time. An attached laptop computer was used to record the spectral data.

Bead Transplantation

Mice were anesthetized with an intraperitoneal injection of 50 mg/kg b.w. sodium pentobarbital (Abbot Laboratories, Chicago, IL). An incision was made above either the kidney or liver, as in the islet transplantations. The luminescent bead was glued onto the kidney or liver at the site of islet engraftment using Vetbond™ tissue adhesive (3M, St. Paul, Minnesota). The incision was closed with subcutaneous sutures and skin staples as before.

Imaging of Luminescent Beads

Imaging of luminescent beads was carried out using the charge coupled device (CCD) camera used for islet imaging. Beads were placed on a black felt pad within the light tight box. A background image of 1 ms was taken for background noise subtraction. Beads were then imaged with a 1 second exposure time. Beads were re-imaged 4 times, reorienting the bead between each image, in order to quantify variability in bead light emission. Bead luminescence was quantified using Metamorph software. Equal area regions were drawn around the beads and photon count was quantified by summing pixel intensities within the region. After bead implantation each mouse was imaged weekly for 6 weeks. A one second exposure was used for all bead images. Implanted bead luminescence was quantified by photon counting, as in the islet experiments. Spot size was determined using Metamorph. The maximum intensity pixel from each implanted bead was found and measured. A threshold was then applied at half the maximum intensity for all pixels above that value. The number of pixels exceeding threshold was determined. This area is the spot size; full width at half maximum (FWHM) was calculated as the diameter of this circular spot size.

$$FWHM = \sqrt{\frac{4 \cdot Area_{threshold}}{\pi}} \tag{15}$$

Rotational Variability Study

The rotational variation in implanted bead intensity was measured using a rotational stage. This stage consisted of a hinged black felt platform that allowed 50 degree rotation in

either direction (Figure 1). Mice with luminescent beads were attached to the stage using Velcro and placed in the light tight imaging box of the CCD camera. Mice with the bead on the renal capsule were placed in a lateral decubitis position (bead facing up); mice with hepatic beads were placed in the supine position. The stage was rotated in ten degree increments from –50 degrees to 50 degrees (with 0 degrees indicating parallel to the floor). Positive rotation was defined as clockwise rotation when viewed from the head of the mouse. Thus for renal beads positive rotation was defined as rotation toward the prone orientation, while negative rotation indicated rotation towards the supine orientation. One-second camera exposures were taken at each angle. Luminescence was quantified using Metamorph's photon counting, as previously described. Luminescence at each angle was normalized to light intensity at 0 degrees.

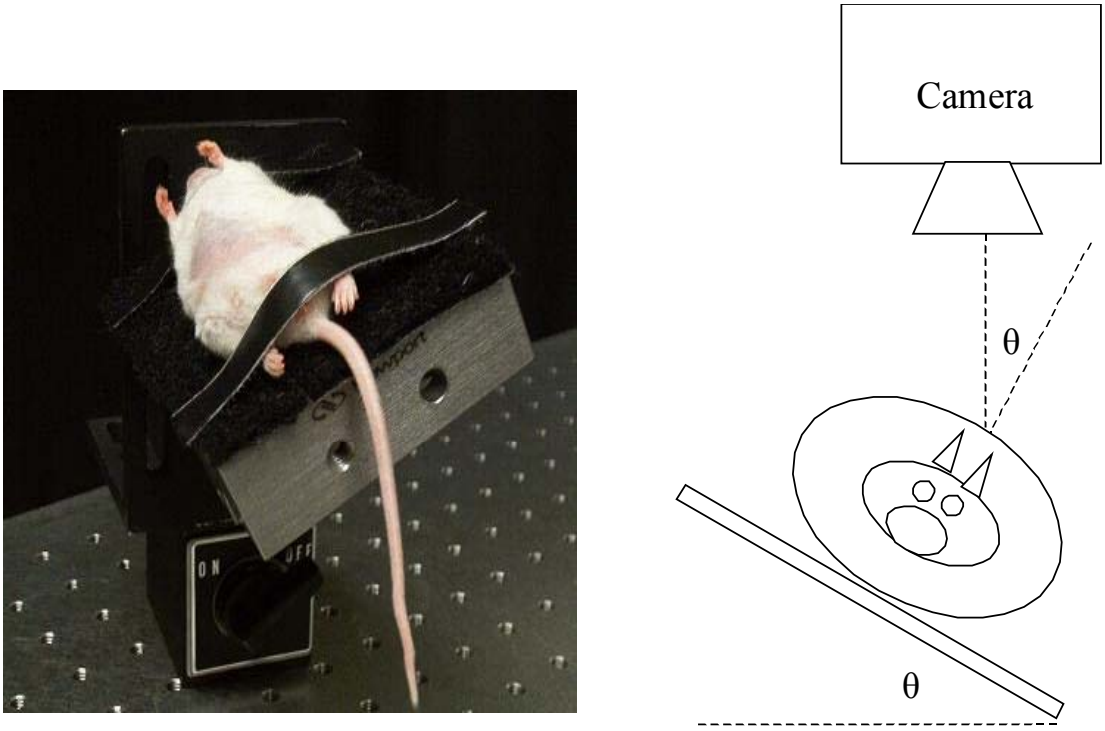

Figure 1: Image and schematic of a mouse with a hepatic bead on the rotational stage. Mice were attached rigidly to the stage via Velcro. The stage could then be rotated with respect to the camera axis 50 degrees from flat in either direction. Ten-degree increments were marked beneath the stage to delineate the angle of rotation.

Monte Carlo Simulation

Monte Carlo simulation was used to model the propagation of photons from the luminescent bead to the aperture of the CCD camera. Monte Carlo simulation provides a well-accepted numerical simulation of light transport in multi-layer tissues close to tissue boundaries [36]. Transmission of light through the tissue was determined as a function of radial position; photon transmission reaching the camera aperture was calculated as the photon weight transmitted within the radius of the camera aperture. Monte Carlo simulation was run for three conditions: the bead alone, the bead implanted in the renal capsule, and the bead implanted beneath the liver. The bead simulation consisted of a single layer of non-absorbing, non-scattering media corresponding to the air between the camera stage and aperture. The renal bead simulation added a layer of skin to the air layer. The hepatic bead simulation added a layer of liver tissue to the skin and air layers for a three-layer model. Thickness of the tissue layers was determined by sacrificing the animal and measuring tissue thickness overlying the bead using calipers.

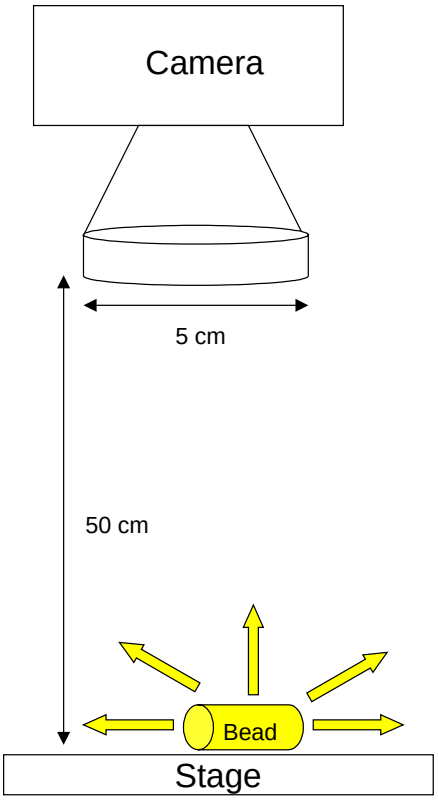

Figure 2. Schematic of geometry used in Monte Carlo simulations. The luminescent bead was modeled as an isotropic light source. A 50 cm gap of air separated this light source from the camera. Light transmission was summed for photons reaching the inner 2.5 cm radius corresponding to the camera aperture.

Table 1. Optical properties used in Monte Carlo simulations. Simulation of the bead alone consisted of a single layer model consisting of only the air layer between the camera stage and aperture. Simulation of the renal bead consisted of the skin layer overlaying the bead and the air layer. Simulation of the hepatic bead used the three-layer model including optical properties of the liver overlying the bead, as well as the skin and air layers.

	Thickness [cm]	n	g	μ_a [cm^{-1}]	μ_s [cm^{-1}]
Air	50	1	1	1E-09	0
Skin	0.025	1.37	0.9	1	90
Liver	0.1	1.37	0.9	9.6	89

Results

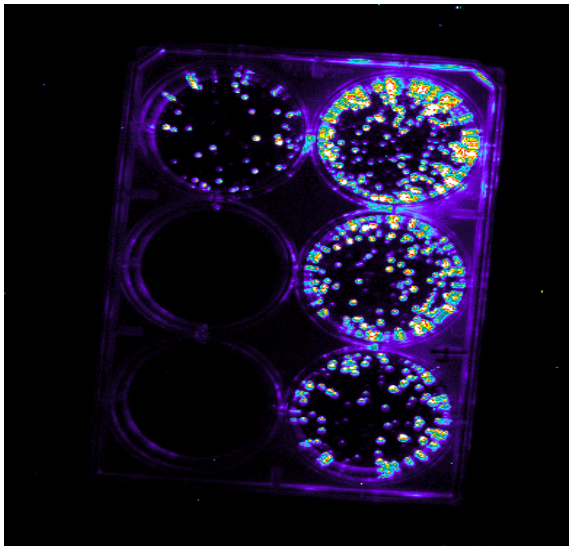

Figure 3: Image of bioluminescent human islets in a 6-well plate. The plates contain (clockwise from lower left): 1000 islets with no virus, 0 islets, 50 islets, 1000 islets, 500 islets, and 100 islets. Image was taken with a CCD camera with a four-minute exposure time and binning of 2.

Bioluminescent Islets

Bioluminescent islets can be imaged in vitro using an ultra-sensitive CCD camera for photon detection. Addition of the substrate luciferin to islets expressing luciferase induces bioluminescence (Figure 2). Bioluminescence intensity increases as the quantity of islets in the well plate increases. This bioluminescence can be quantified by photon counting of the glowing area. As shown in Figure 3, islet bioluminescence correlates linearly to islet number in vitro.

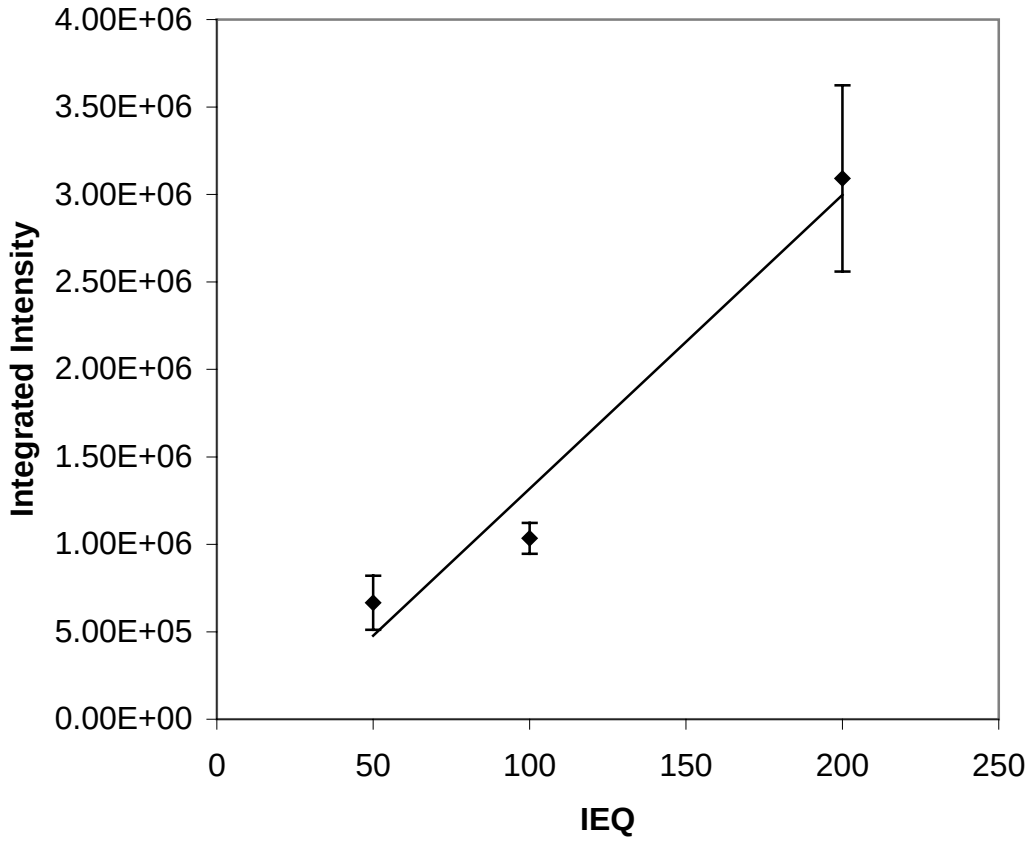

Figure 4: Plot of bioluminescent intensity of in vitro murine islets in a 6-well plate. Image was taken with a CCD camera with a four-minute exposure time and binning of 5. The coefficient of determination (R^2) is 0.9636. Shown is the mean of 4 wells for each islet number plus or minus the standard error of the mean.

Bioluminescent islets transplanted beneath the renal capsule of NOD-SCID mice can be imaged using a CCD camera. Intraperitoneal injection of the substrate luciferin into mice bearing bioluminescent islets induces bioluminescence detectable from outside the mouse. This luminescence can then be quantified using photon counting of the glowing region. Bioluminescence intensity correlates linearly to the number of islets transplanted (Figure 4).

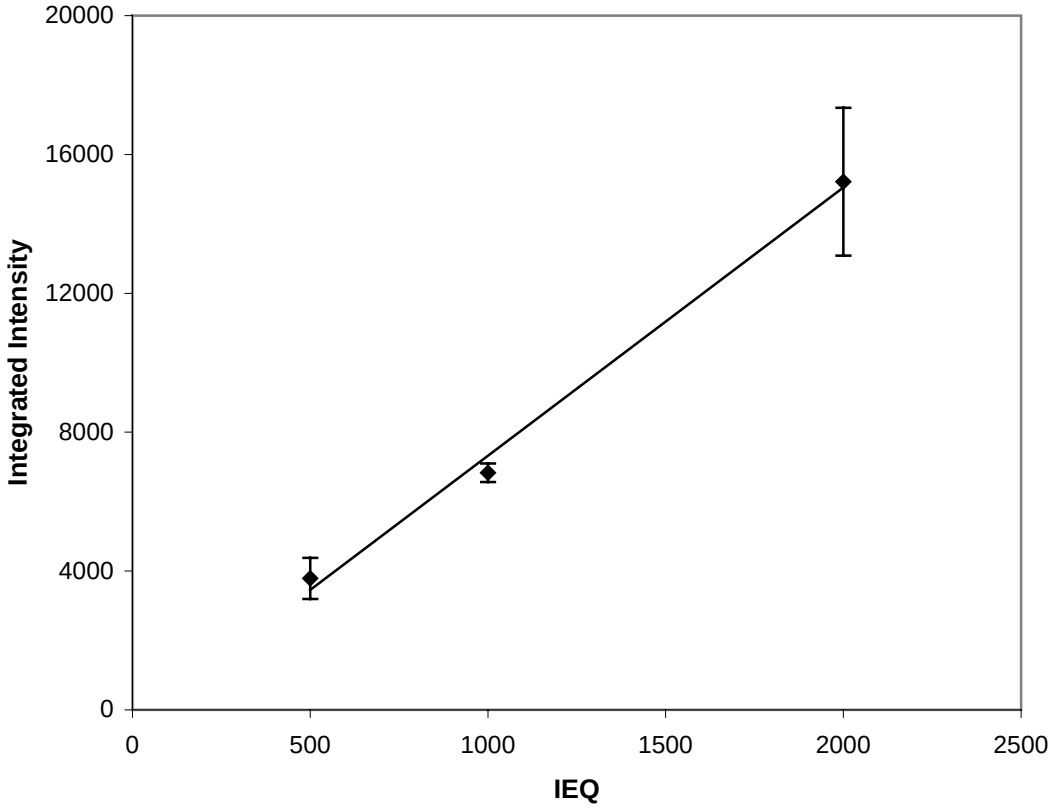

Figure 5: Plot of transplanted islet equivalency (IEQ) vs. bioluminescence intensity. Mice were transplanted with human islets (courtesy of NIH islet isolation facility) under the renal capsule. Images were taken 4 weeks post transplantation. Image was taken with a CCD camera with a four-minute exposure time and binning of 5. Shown is the mean of 3 or 4 mice at each islet number plus or minus the standard deviation. The coefficient of determination (R^2) is 0.9946.

Two different anatomical sites are typically used for murine islet transplantation. Islets transplanted beneath the renal capsule form a stable islet graft in a small area. However, liver transplantation is more applicable to clinical studies, as the liver is the site of human islet transplantations. Islets transplanted into the renal capsule undergo different optical interactions than those transplanted into the liver. As seen in Figure 5, light emission from hepatic islets is significantly less than that from renal islets. Light traveling from the liver must penetrate through more tissue than light propagating from the kidney.

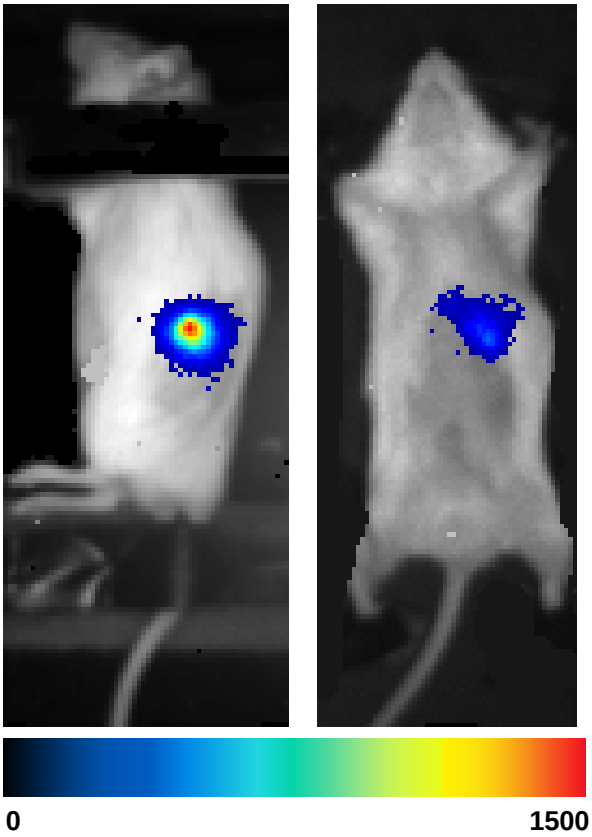

Figure 6: Image of mice with 100 transplanted bioluminescent islets. Image was taken with a CCD camera with a four-minute exposure time and binning of 5. The mouse on the left was transplanted with 100 murine islets under the renal capsule. The mouse on the right was transplanted with murine 100 islets into the portal vein. Both mice were imaged two weeks post transplantation.

Luminescent Beads

Luminescent beads provide a constant light source with a half live of 10 years. These luminescent beads were imaged in a CCD camera (Figure 6). Light emission from these beads was quantified using photon counting. The spectral emission of these beads was found using a fiber optic probe attached to a spectrometer. As seen in Figure 7, the spectral emission of the luminescent beads is similar to that of the luciferase reaction. The luminescent bead shows peak emission at 600 nm, slightly higher than the 563 nm peak emitted by the luciferase reaction. But the bead spectrum provides a good replica of the luciferase reaction.

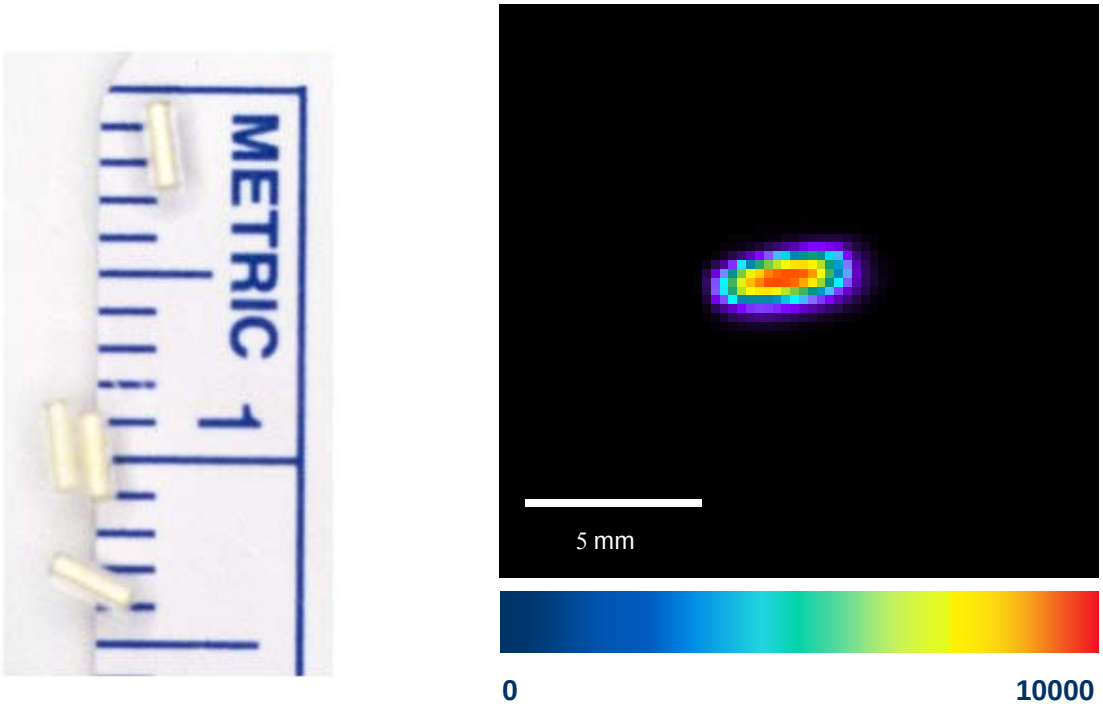

Figure 7: Image of luminescent beads prior to implantation. The left panel shows the scale of the beads. The image in the right panel was taken with a CCD camera with a one second exposure time. The units of the scale bar are photon counts per pixel.

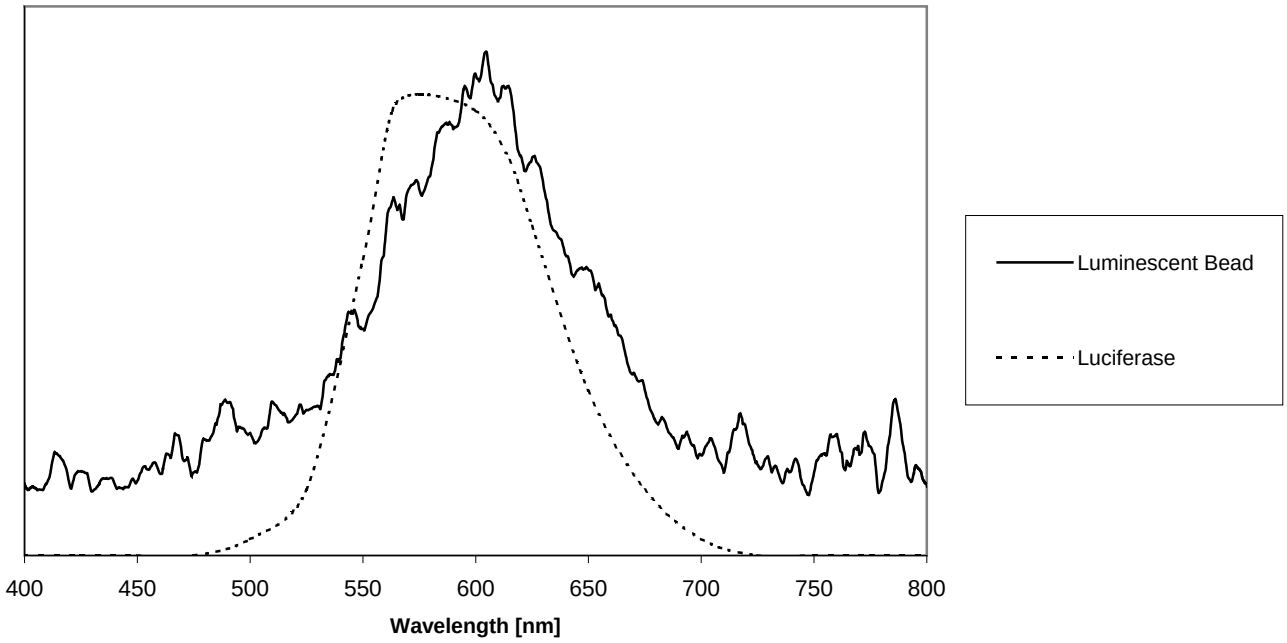

Figure 8: Spectra of luminescent bead prior to implantation and the luciferase reaction. The spectral emission of these beads was measured using a fiber optic probe attached to a spectrometer (Ocean Optics Inc., Dunedin, FL) with one-second integration time. The spectral emission of luciferase was plotted from commonly accepted data [30].

Luminescent beads were implanted at the sites used for islet transplantation: at the renal capsule and underneath the frontal lobe of the liver. Figure 8 shows a luminescent bead implanted at the renal capsule (left) and underneath the frontal lobe of the liver (right). The renal bead shows a brighter, more concise region of luminescence. Light emission from the hepatic bead is less bright and more diffuse. Note the difference in scale between the two images.

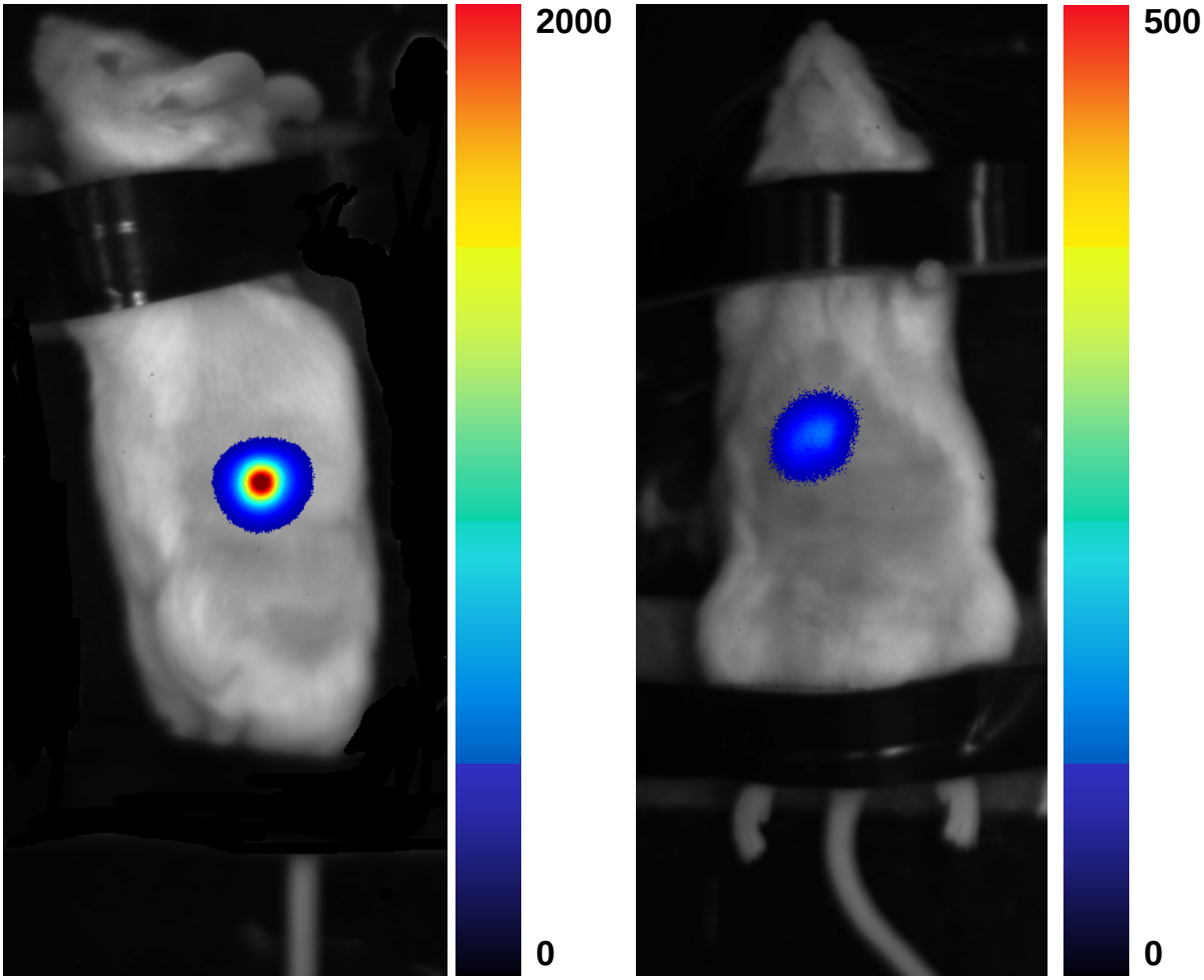

Figure 9: Image of luminescent bead implanted at the renal capsule (left) and underneath the frontal lobe of the liver (right). Note the differences in scale. Image was taken with a CCD camera with a one second exposure time.

Mice with luminescent beads implanted at the renal capsule were imaged weekly for 6 weeks to determine the temporal variation in luminescence intensity. At one-week post implantation, the mice with renal beads showed significantly lower luminescence than in latter weeks (t test, $\alpha = 0.05$). By 6 weeks post implantation luminescence had more than doubled. Six weeks post transplantation the ratio of bead luminescence while implanted to bead luminescence pre-implantation was 0.2394 +/- 0.0261. The renal beads also showed more variation in the week immediately post operation. By the second week post implantation this variation had decreased by 45%.

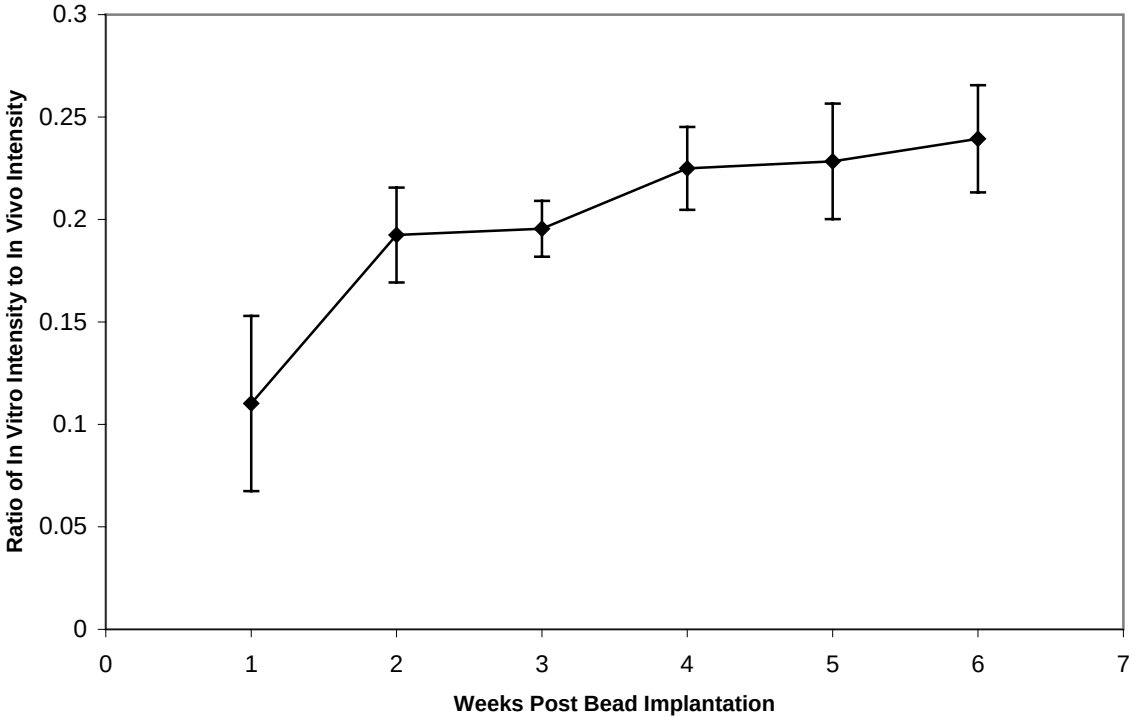

Figure 10: Intensity of luminescent beads implanted in the renal capsule as a function of time. Luminescence intensity was measured using a CCD camera (Roper Scientific, Trenton, NJ) with a one second exposure time. Intensity is expressed as the ratio of bead intensity when implanted to the bead intensity pre-implantation. Mice were imaged weekly following bead implantation. Shown are the mean and standard error of the mean of 4 mice.

Luminescent beads implanted beneath the liver showed a similar pattern temporally. The first week luminescence was lower than latter weeks. By the sixth week, the ratio of hepatic bead intensity to bead intensity pre-implantation had reached a steady state value of 0.0645 +/- 0.0140.

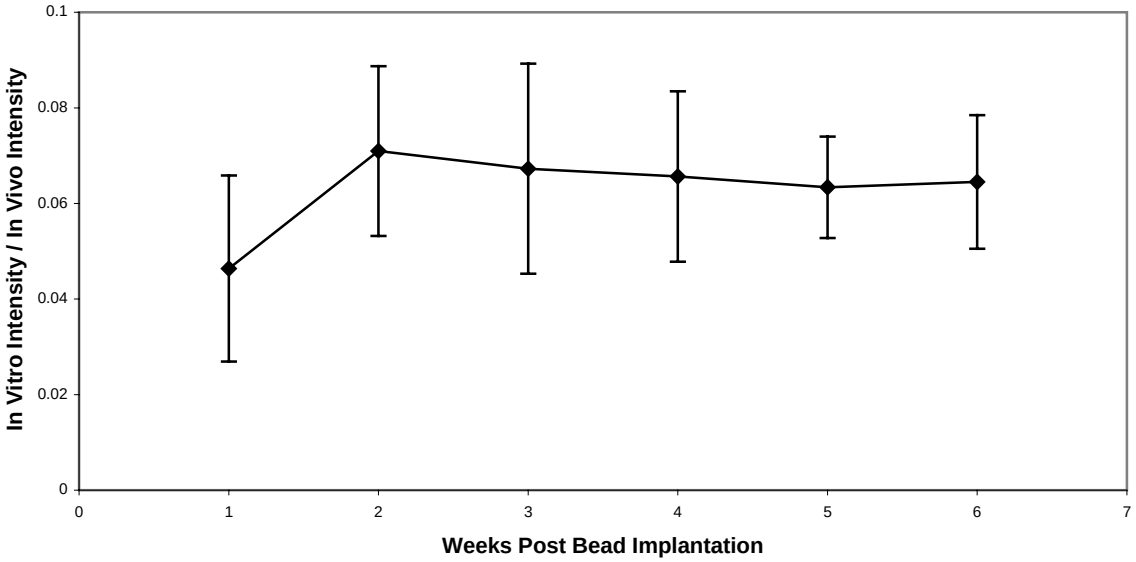

Figure 11: Intensity of luminescent beads implanted beneath the liver as a function of time. Luminescence intensity was measured using a CCD camera (Roper Scientific, Trenton, NJ) with a one second exposure time. Intensity is expressed as the ratio of bead intensity when implanted to the bead intensity pre-implantation. Mice were imaged weekly following bead implantation. Shown are the mean and standard error of the mean of 3 mice.

The luminescence from the renal and hepatic implanted beads was also analyzed for light scattering. Spot size, full width at half maximum (FWHM), was determined at each week post implantation. The beads implanted under the liver showed a greater spot size at each week (Figure 11). By the sixth week post implantation, the FWHM of the liver implanted beads were 17% higher than the FWHM of the renal beads. As in the intensity measurements, the greatest variability was seen one week following surgery.

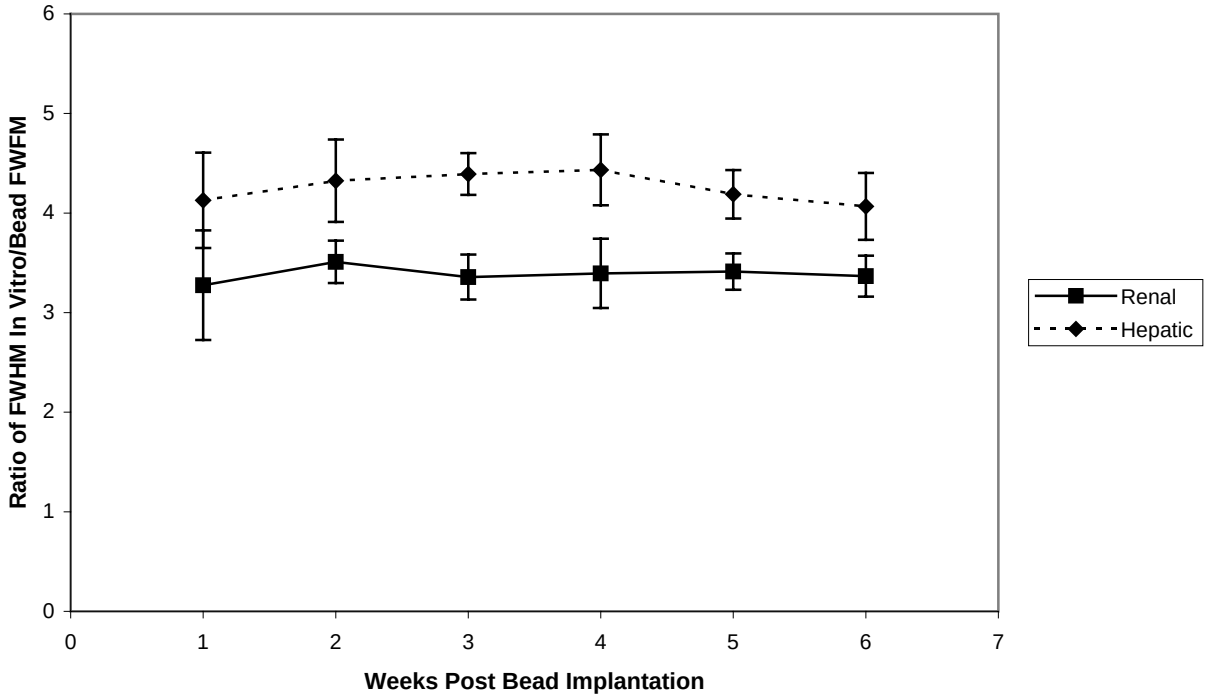

Figure 12: Spot size of luminescent beads implanted in the renal capsule and beneath the liver as a function of time after implantation. Spot size was measured using a CCD camera (Roper Scientific, Trenton, NJ) with a one second exposure time. The maximum intensity pixel of each implanted bead was found using Metamorph (Version 4.6r6, Universal Imaging Corporation, Downingtown, PA). A threshold at half of this maximum was applied for each implanted bead and area of threshold was measured using Metamorph. The diameter of this circular spot size was calculated as full width half maximum (FWHM). Spot size is expressed as the ratio of FWHM when implanted to the FWHM of the bead pre-implantation. Mice were imaged weekly following bead implantation. Shown are the mean and standard error of the mean of the renal capsule and hepatic mice, n = 4 and n = 3, respectively.

Monte Carlo Simulation

Light propagation from the luminescent bead to the camera aperture was modeled using Monte Carlo simulation. Simulation was run for the bead alone, for the bead implanted on the renal capsule, and for the bead implanted beneath the renal capsule. The results of this simulation are shown in Table 2. These results were compared to the experimental results of the bead implantations 6 weeks post implantation. The two values show excellent correlation.

Table 2: Monte Carlo simulation of light propagation from the luminescent bead. Light transmission through all tissue (and air) layers was calculated as a function of radial position. Photon transmission at radii less then or equal to the radius of the camera aperture was summed to yield total photons reaching the camera. These photon transmission values were used to calculate the ratio between the renal bead and bead pre-implantation, as well as the ratio between the hepatic bead and bead pre-implantation. These values are shown along with the ratio between in vivo and in vitro bead luminescence found experimentally.

	Monte Carlo Simulation	Bioluminescent Imaging 6 Weeks Post Implantation
Ratio of Renal Bead Intensity to Bead Pre-Implantation	0.2860	0.2394+/- 0.0261
Ratio of Hepatic Bead Intensity to Bead Pre-Implantation	0.0495	0.0645 +/- 0.0140

Rotational Variation

The luminescence emitted from the implanted beads was also analyzed for rotational variation. As shown in Figures 12 and 13, the luminescence intensity measured by the CCD camera changed as a function of rotational angle. As the mouse was rotated from a flat position (lateral for renal beads, supine for hepatic beads) the luminescence intensity decreased. At low angles, intensity decreased only slightly. But at 50-degree rotation from flat, luminescence intensity decreased to approximately 0.27 of the flat intensity for the renal bead and 0.48 of the flat intensity for the hepatic bead. The rotational variation was more pronounced for beads at the renal capsule than for hepatic beads.

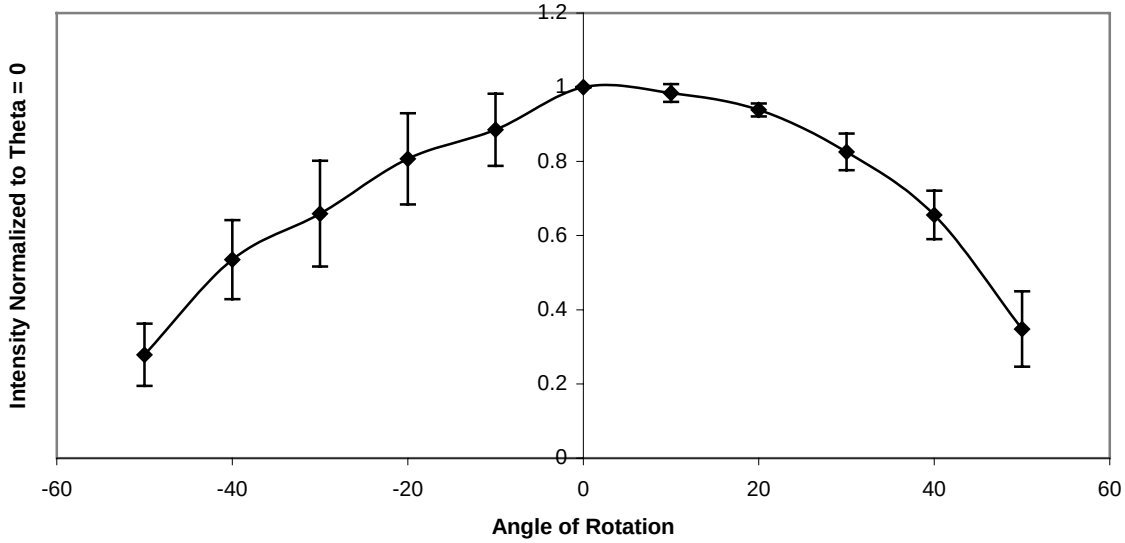

Figure 13: Intensity of luminescent beads implanted in the renal capsule as a function of position. Mice were placed laterally, with the implanted bead facing up, on a rotational stage. The stage was rotated in 10-degree increments from –50 degrees to 50 degrees. Luminescence intensity was measured using a CCD camera (Roper Scientific, Trenton, NJ) with a one second exposure time at each angle. Intensities were normalized to the intensity of each mouse when laying flat (angle of rotation = 0). Shown are the mean and standard error of the mean for 4 mice.

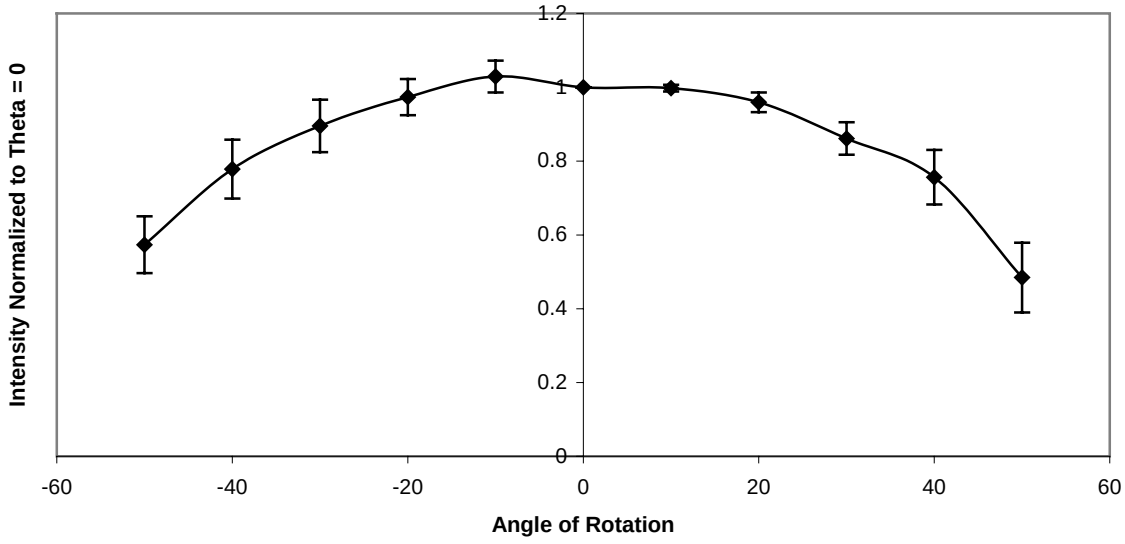

Figure 14: Intensity of luminescent beads implanted beneath the liver as a function of position. Mice were placed supine on a rotational stage and rotated in 10-degree increments from –50 degrees to 50 degrees. Luminescence intensity was measured using a CCD camera with a one second exposure time at each angle. Intensities were normalized to the intensity of each mouse when laying flat (angle of rotation = 0). Shown are the mean and standard error of the mean for 3 mice.

Discussion

This study examines the use of in vivo bioluminescence imaging (BLI) for tracking transplanted pancreatic islets. Islets infected with an adenovirus carrying the constitutively expressed reporter gene luciferase emit light when combined with the substrate luciferin. This luminescence can be quantified using photon-counting measurements. For a given set of transfection conditions, a linear relationship exists between the number of islets transplanted and the measured light produced by the bioluminescence reaction. Transplanted islets can also be imaged *in vivo* even from deep tissues in small animals, showing distinct bioluminescent regions corresponding to the area of islet graft. Quantification of photon emission *in vivo* shows a linear relationship between numbers of islets transplanted and light emission.

The linear relationship between number of bioluminescent islets and emitted light intensity is useful for comparing sets of transplants. However, it is not necessarily applicable across studies in which imaging parameters and transfection efficiency may vary. The measured light intensity depends on the transfection efficiency of the adenovirus, the size of the islets, and the parameters used in imaging, such as integration time and are of the integration region. The parameter of interest when tracking transplanted islets is the number of islets surviving post-transplantation. The correlation of light emission to islet number *in vivo* enables the use of IBL as a non-invasive means of islet assessment in mouse models of diabetes and islet transplants. In turn, these models may be used as high throughput models for assessment and screening of novel therapeutic procedures aimed at increasing functional islet survival. While relative information regarding islet mass or numbers as function of time or in response to pharmacological intervention is readily obtained from the bioluminescence measurements (i.e. increase or decrease of signal), absolute information regarding the number or percentage of islets surviving requires more detailed investigation of the optics governing light transmission from the bioluminescent source to the CCD camera aperture.

In order to model bioluminescence from islet grafts, luminescent beads were employed. These beads were implanted at the two common sites of islet transplantation: the renal capsule and liver. The implanted beads mimic bioluminescence with constant and known intensity light emission from the site of islet grafts.

As expected, light emitted from islet grafts is significantly lower than light emission from islets *in vitro*. However, it was previously unclear how much of this decrease in luminescence

was due to islet death post-transplantation and how much could be attributed to light attenuation by tissues overlying the implants. Comparison of renal grafts to hepatic grafts shows a discrepancy between light transmission from each site. Renal transplants are brighter and spatially more concise. Transplantations into the liver are less bright and more diffuse. The renal capsule implantation site is more superficial; the mean free path of light emitted from this site is shorter than light emitted from the liver. Light emanating from the hepatic transplants must pass through liver tissue, a highly perfused tissue that contributes significant light scattering and absorption. The light emitting beads transplanted at the site of islet grafts were used to quantify light transmission through the tissues overlying the luminescent source. For renal implantation, the ratio between luminescence after implantation to luminescence of the bead alone stabilized to a constant value six weeks post-implantation. This ratio was found to be 0.2394+/- 0.0261. Monte Carlo simulation of light transmission to the CCD camera yields an *in vivo* to *in vitro* ratio of 0.2744. For hepatic implantation the ratio of light intensity from the liver bead to the bead alone was 0.0645 +/- 0.0140 six weeks post surgery. Monte Carlo simulation of hepatic light transmission yields a ratio of 0.0667. Experimental results for both renal and hepatic implanted beads are in good agreement with Monte Carlo modeling of photon propagation. Light attenuation by tissue overlying hepatic transplants results in nearly four-fold less light transmission from hepatic islets than renal islets. This ratio between *in vivo* and *in vitro* luminescence found using the constant intensity luminescent beads could then be compared to the ratio between islet bioluminescence *in vivo* and *in vitro*. Preliminary results indicate that the ratio for islets is much lower, indicating a large (six to eight fold) drop in viable islets post transplantation.

The luminescence from implanted beads was tracked temporally to investigate time dependent effects on light transmission. Islets studies previously showed that transplanted bioluminescent islets show lower luminescence the week immediately following surgery. The exact reason for this lower light emission was unknown. It was thought that insufficient vascularization of the islets one-week post-op could hamper delivery of the substrate luciferin to the islet graft. Scar tissue from suturing and stapling the skin overlying the islet grafts was also believed to absorb and scatter bioluminescence. This affect of the inflammatory response on bioluminescence measurements is dynamic immediately post op as the wound healing process rapidly progresses. One to two weeks post implantation the attenuation by scar tissue reaches a

steady state as the wound heals. Results from the bead implantations indicate that the latter explanation of low luminescence immediately following surgery is responsible. Scar tissue above the luminescent source attenuates light transmission from the light source. The mice with beads implanted at both the renal capsule and liver show lower luminescence the first week post transplantation. Additionally, they show greatest variation in light transmission at one-week post implantation, a pattern repeated with the islet transplants.

The spot size of luminescence differs between hepatic islets and renal islets. Islets infused into the portal vein typically embolize throughout the liver, leading to a more diffuse light source. Renal islets are typically isolated in a contiguous graft. However, spot size is also a function of the tissue optics through which propagating photons pass. Bioluminescence from the liver passes through hepatic tissue, leading to higher scattering and thus a larger spot size than renal grafts. The extent to which increased hepatic light scattering leads to larger spot size was analyzed using the mice with implanted beads. The full width at half maximum (FWHM) for the hepatic beads was 17% higher than the renal bead implants. The islet transplants show a much larger spot for liver placement relative to renal, suggesting that (as expected) the liver islets are more spatially dispersed throughout the organ versus the renal capsule where the graft is clustered together.

Bioluminescence measurements can be affected by rotation of the sample. Detected photon emission depends on the angle of the surface normal makes with the optical axis of the camera system. Presumably the primary reason for this is the fact that light emission from a highly scattering medium resembles a Lambertian distribution with most of the light emitting in an angle normal to the surface [37]. The practical implication of this finding is that the exact positioning of the mouse relative to the camera axis is an important parameter that must be controlled carefully. Failure to do so can induce variations in the photon counting measurements from one time point to the next that are not representative of the biological processes for which bioluminescence is the surrogate marker. The application of tomographic analysis to bioluminescence imaging, thus far still in a developmental state, must take into account these rotational effects. The effect of rotation on luminescence measurements was determined for both renal and hepatic implanted beads. At small angles, rotation had little affect on photon counting. However, at rotations of 50 degrees from flat, measured luminescence decreased to a third of the flat measurement for renal beads. For hepatic beads, the decrease at 50 degrees from flat was

slight less, but still resulted in measured intensity less than half of the flat. Both implantation sites showed a parabolic relationship between angle and luminescence, with luminescence decreasing with increasing angle from flat. However, the drop in renal intensity was sharper and more pronounced than that seen from the hepatic bead. The hepatic bead implantation is imaged with a supine position indicating flat. The renal bead was imaged with a lateral placement serving as flat. Both of these placements were used to minimize the mean free path of light through tissue. The supine placement has a much larger flat surface, while the lateral placement is subject to sharper curvature. The liver bead thus has more surface area normal to the camera axis than the renal bead. This results in a slower drop in luminescence with increasing rotation for the hepatic implantation.

Conclusions

Bioluminescence imaging can be used to non-invasively monitor transplanted pancreatic islets *in vivo*. A linear relationship exists between number of luminescent islets and integrated photon counts *in vitro*. This linear relationship holds for islets transplanted beneath the renal capsule, as well. To fully utilize bioluminescence imaging as a modality for imaging transplanted islets, light intensity can be related to number of islets surviving post transplantation. This requires investigation of the optical properties of tissue overlying the site of transplantation.

Models of bioluminescence using constant light emission sources can yield critical information regarding light emission. The attenuation of light by tissues overlying the renal capsule and hepatic islet transplantations was quantified. Light emission from the renal capsule was approximately four times greater than light emission from a hepatic source. The ratios of *in vivo* to *in vitro* luminescence found experimentally are in excellent agreement with Monte Carlo simulation of photon migration. These ratios can be used, along with bioluminescence measurements of islets *in vitro* and *in vivo*, to correlate photon counting measurements to actual islet number surviving post-transplantation.

Surgical artifacts can affect bioluminescence measurements. Light emission the week immediately following surgery can be significantly lower than latter weeks due to post-surgical inflammation and scarring. Scar tissue from sutures and surgical staples attenuates light more strongly than native skin, leading to lower measured bioluminescence. This finding indicates

that bioluminescence imaging may not accurately reflect islet mass until two weeks post transplantation.

The spot size of light emission differs for renal and hepatic light sources. Hepatic sources traverse highly vascular liver tissue, leading to higher scattering. This results in spot size, measured as full width at half maximum, larger for hepatic sources. However, the increase in hepatic spot size determined using luminescent bead was not as great as the increase in spot size between renal and hepatic islets, indicative of the dispersed nature of hepatic islet grafts.

Bioluminescence measurements are affected by the orientation of the subject. Rotation of the subject can lead to decreased photon-counting measurements. This finding has application in everyday bioluminescence imaging, as subjects can exhibit motion artifacts during imaging, as well as development of tomographic bioluminescence imaging systems. The rate of light intensity decrease with rotation angle is dependent on the source of luminescence. Light projected on a flat surface undergoes less light decrease with rotation than surfaces with sharp curvature.

Bioluminescence measurements are subject to some inherent limitations. *In vivo* BLI can be applied only to small animal models; the tissue thickness of primate models prevents BLI studies. Additionally, the islets constitutively express the reporter gene luciferase in all islet cells, not just β-cells. In most islet transplantation studies, only the insulin producing β-cells are of interest. The study is also subject to some limitations of the adenovirus system used for islet transfection. Dividing cells currently do not receive the transgene; use of an AAV system will permit tracking of cell replication.

CHAPTER III

FUTURE WORK

Future work will incorporate measurements made using the constant light emission models of islet bioluminescence to correlate photon-counting measurements of islets to the islet number surviving post-transplantation. This will yield insight into the fate and survival rate of transplanted islets. A number of interventions will be introduced to islet transplant recipients; their effects can be quantified by bioluminescence measurements.

We are also currently working on the development and characterization of two transgenic mouse models. The first expresses the reporter gene luciferase under control of the PDX-1 promoter, a beta cell specific marker. The second is also beta-cell specific, expressing luciferase under control of the insulin promoter. These transgenic mouse models will express luciferase solely in the beta cells, rather than throughout the islet. This will allow non-invasive measurement of beta cell mass specifically, rather than islet mass as a whole.

Results from the rotational experiments will be correlated to measurements of surface normals. Surface normals can be found using a laser range scanner; they are expected to correlate to bioluminescence measurements as a function of angle of rotation. This information can be applied to tomographic bioluminescence imaging.

Bioluminescence imaging will also be co-registered to other imaging modalities. Pilot studies have shown that the luminescent beads used in this study can be imaged in a phantom in an MR scanner. Co-registration between imaging modalities can combine gene specific bioluminescence with the superior spatial resolution offered by MRI. Integration of the two modalities can enhance the potential of *in vivo* bioluminescence imaging (BLI). We are also developing multi modality probes (rfp-luc-tk) which can be used in confocal microscopy, and IBL, as well as PET [38].

REFERENCES

1. Shapiro, A.M.J., et al., Islet transplantation in seven patients with type 1 diabetes mellitus using a glucocorticoid-free immunosuppressive regimen. New England Journal of Medicine, 2000. 343(4): p. 230-238.

2. Lakey, J.R., P.W. Burridge, and A.M. Shapiro, Technical aspects of islet preparation and transplantation. Transpl Int, 2003. 16(9): p. 613-32.

3. von Mering, J. and O. Minkowski, Diabetes mellitus after pancreas extirpation. Archiv fur Exper Path und Pharmakol, 1889. 26: p. 111.

4. Minkowski, O., Weitere Mitteilungen uber den diabetes mellitus nach extirpation des pancreas. Berl Klin Wochenschr, 1892. 2: p. 1303.

5. Williams, P., Notes on diabetes treated with extract and by grafts of sheep's pancreas. Br Med J, 1894. 2: p. 1303.

6. Banting, F., et al., Pancreatic extracts in the treatment of diabetes mellitus: preliminary report. Can Med Assoc J, 1922. 12: p. 141.

7. Kelly, W.D., et al., Allotransplantation of the pancreas and duodenum along with the kidney in diabetic nephropathy. Surgery, 1967. 61(6): p. 827-37.

8. Robertson, R.P. and D.E. Sutherland, Pancreas transplantation as therapy for diabetes mellitus. Annu Rev Med, 1992. 43: p. 395-415.

9. Robertson, R.P., et al., Pancreas and islet transplantation for patients with diabetes. Diabetes Care, 2000. 23(1): p. 112-6.

10. Navarro, X., D.E. Sutherland, and W.R. Kennedy, Long-term effects of pancreatic transplantation on diabetic neuropathy. Ann Neurol, 1997. 42(5): p. 727-36.

11. Fioretto, P., et al., Reversal of lesions of diabetic nephropathy after pancreas transplantation. N Engl J Med, 1998. 339(2): p. 69-75.

12. Gross, C.R., et al., Impact of transplantation on quality of life in patients with diabetes and renal dysfunction. Transplantation, 2000. 70(12): p. 1736-46.

13. Robertson, R.P., Pancreas transplantation in humans with diabetes mellitus. Diabetes, 1991. 40(9): p. 1085-9.

14. Hirshberg, B., et al., State of the art: islet transplantation for the cure of type 1 diabetes mellitus. Rev Endocr Metab Disord, 2003. 4(4): p. 381-9.

15. Ballinger, W.F. and P.E. Lacy, Transplantation of intact pancreatic islets in rats. Surgery, 1972. 72(2): p. 175-86.

16. Najarian, J.S., et al., Human islet transplantation: a preliminary report. Transplant Proc, 1977. 9(1): p. 233-6.

17. Najarian, J.S., et al., Total or near total pancreatectomy and islet autotransplantation for treatment of chronic pancreatitis. Ann Surg, 1980. 192(4): p. 526-42.

18. Robertson, R.P., et al., Prevention of diabetes for up to 13 years by autoislet transplantation after pancreatectomy for chronic pancreatitis. Diabetes, 2001. 50(1): p. 47-50.

19. Brendel, M., International Islet Transplant Registry Newsletter #9. 2001.

20. Drachenberg, C.B., et al., Islet cell damage associated with tacrolimus and cyclosporine: morphological features in pancreas allograft biopsies and clinical correlation. Transplantation, 1999. 68(3): p. 396-402.

21. Shapiro, A.M., C. Ricordi, and B. Hering, Edmonton's islet success has indeed been replicated elsewhere. Lancet, 2003. 362(9391): p. 1242.

22. Greer, L.F., 3rd and A.A. Szalay, Imaging of light emission from the expression of luciferases in living cells and organisms: a review. Luminescence, 2002. 17(1): p. 43-74.

23. Gould, S.J. and S. Subramani, Firefly luciferase as a tool in molecular and cell biology. Anal Biochem, 1988. 175(1): p. 5-13.

24. Nguyen, V.T., M. Morange, and O. Bensaude, Firefly luciferase luminescence assays using scintillation counters for quantitation in transfected mammalian cells. Anal Biochem, 1988. 171(2): p. 404-8.

25. Brasier, A.R., J.E. Tate, and J.F. Habener, Optimized use of the firefly luciferase assay as a reporter gene in mammalian cell lines. Biotechniques, 1989. 7(10): p. 1116-22.

26. Gates, B.J. and M. DeLuca, The production of oxyluciferin during the firefly luciferase light reaction. Arch Biochem Biophys, 1975. 169(2): p. 616-21.

27. de Wet, J.R., et al., Firefly luciferase gene: structure and expression in mammalian cells. Mol Cell Biol, 1987. 7(2): p. 725-37.

28. Keller, G.A., et al., Firefly luciferase is targeted to peroxisomes in mammalian cells. Proc Natl Acad Sci U S A, 1987. 84(10): p. 3264-8.

29. Wood, K.V. and M. DeLuca, Photographic detection of luminescence in Escherichia coli containing the gene for firefly luciferase. Anal Biochem, 1987. 161(2): p. 501-7.

30. Rice, B.W., M.D. Cable, and M.B. Nelson, In vivo imaging of light-emitting probes. J Biomed Opt, 2001. 6(4): p. 432-40.

31. Contag, C.H., et al., Visualizing gene expression in living mammals using a bioluminescent reporter. Photochem Photobiol, 1997. 66(4): p. 523-31.

32. Rehemtulla, A., et al., Rapid and quantitative assessment of cancer treatment response using in vivo bioluminescence imaging. Neoplasia, 2000. 2(6): p. 491-5.

33. Welch, A.J. and M.J.C. van Gemert, Optical-Thermal Respoonse of Laser-Irradiated Tissue. Lasers, Photonics, and Electro-Optics, ed. H. Kogelnik. 1995, New York: Plenum Press.

34. Profio, A.E., L.R. Wudl, and J. Sarnaik, Dosimetry Methods in Photoradiation Therapy. Advances in Experimental Medicine and Biology, 1985. 193: p. 35-41.

35. Zhu, D., Q. Luo, and J. Cen, Effects of dehydration on the optical properties of in vitro porcine liver. Lasers Surg Med, 2003. 33(4): p. 226-31.

36. Wang, L., S.L. Jacques, and L. Zheng, MCML--Monte Carlo modeling of light transport in multi-layered tissues. Comput Methods Programs Biomed, 1995. 47(2): p. 131-46.

37. Badano, A., et al., Angular dependence of the luminance and contrast in medical monochrome liquid crystal displays. Med Phys, 2003. 30(10): p. 2602-13.

38. Wu, J.C., et al., Molecular imaging of cardiac cell transplantation in living animals using optical bioluminescence and positron emission tomography. Circulation, 2003. 108(11): p. 1302-5.